

Title: Quantum Computation Solves a Half-Century-Old Enigma: Elusive Vibrational States of Magnesium Dimer Found

Short title: Quantum Computation Solves Decades-Old Enigma

Authors: Stephen H. Yuwono¹†, Ilias Magoulas¹†, Piotr Piecuch^{1,2}*

Affiliations

¹Department of Chemistry, Michigan State University, East Lansing, MI 48824, USA.

²Department of Physics and Astronomy, Michigan State University, East Lansing, MI 48824, USA.

†These authors contributed equally to this work.

*Corresponding author. Email: piecuch@chemistry.msu.edu.

15 **Abstract**

5

10

20

25

30

35

40

The high-lying vibrational states of the magnesium dimer (Mg₂), which has been recognized as an important system in studies of ultracold and collisional phenomena, have eluded experimental characterization for half a century. Until now, only the first fourteen vibrational states of Mg₂ have been experimentally resolved, although it has been suggested that the ground-state potential may support five additional levels. Here, we present highly accurate *ab initio* potential energy curves based on state-of-the-art coupled-cluster and full configuration interaction computations for the ground and excited electronic states involved in the experimental investigations of Mg₂. Our ground-state potential unambiguously confirms the existence of nineteen vibrational levels, with ~1 cm⁻¹ root-mean-square deviation between the calculated rovibrational term values and the available experimental as well as experimentally derived data. Our computations reproduce the latest laser-induced fluorescence spectrum and provide guidance for the experimental detection of the previously unresolved vibrational levels.

One Sentence Summary

Quantum computations unravel the mystery of spectral lines that have escaped experimental detection for decades.

MAIN TEXT

INTRODUCTION

The weakly bound alkaline-earth dimers (AE₂) have emerged as probes of fundamental physics relevant to ultracold collisions (*I*), doped helium nanodroplets (*2*), coherent control of binary reactions (*3*), and even fields rarely associated with molecular science, such as optical lattice clocks (*4*) and quantum gravity (*5*). The magnesium dimer is especially important, since it has several desirable characteristics that can be useful in the above applications, such as the absence of hyperfine structure in the most abundant ²⁴Mg isotope which facilitates the analysis of binary collisions involving laser-cooled and trapped atoms, it helps us understand heavier AE₂ diatomics, and, unlike its lighter Be₂ analog, it is non-toxic (*6*). Unfortunately, the status of Mg₂ as a prototype



10

15

20

25

30

35

40

heavier AE₂ species is complicated by the fact that its high-lying vibrational levels and, consequently, the long-range part of its ground-state potential energy curve (PEC) have eluded experimental characterization for half a century. In this regard, the magnesium dimer is even more challenging than its celebrated beryllium counterpart, whose elusive twelfth vibrational level near the dissociation threshold (7, 8), which we also found in (9), was confirmed in 2014 (10) after reanalyzing the spectra obtained in stimulated emission pumping experiments (11).

Experimentally, probing vibrational manifold of the magnesium dimer in its ground, $X^{l}\Sigma_{g}^{+}$, electronic state has to involve excited electronic states, since Mg2, being a homonuclear diatomic, is infrared-inactive. The first high-resolution photoabsorption spectra of Mg2, corresponding to a transition from the ground state to the electronically excited $A^{1}\Sigma_{n}^{+}$ state, were reported in 1970 by Balfour and Douglas (12). Their spectroscopic analysis resulted in 285 G(v'', J'') and 656 G(v', J')rovibrational term values of $^{24}\mathrm{Mg}_2$ involving 13 (v'' = 0–12) $X^1\Sigma_g^+$ and 24 (v' = 1–24) $A^1\Sigma_g^+$ vibrational levels, respectively. Here, we are using the notation in which the vibrational, v, and rotational, J, quantum numbers in the ground electronic state are designated by a double prime, whereas those corresponding to the excited $A^{1}\Sigma_{n}^{+}$ state are marked with a prime. In their pioneering work, Balfour and Douglas constructed a Rydberg-Klein-Rees (13-16) (RKR) $X^{l}\Sigma_{g}^{+}$ PEC in the 3.25–7.16 Å range and located the last experimentally resolved v'' = 12 level about 25 cm⁻¹ below the dissociation threshold, pointing to the existence of extra vibrational states with v'' > 12. It did not take long to detect one of such states. In 1973, Li and Stwalley (17) identified $X^1\Sigma_g^+ \to A^1\Sigma_u^+$ transitions involving the v'' = 13 level in the spectra reported in (12). They accomplished this by extending the original RKR PEC of Balfour and Douglas to the asymptotic region beyond 7.16 Å using theoretical values of C₆ and C₈ van der Waals coefficients (18, 19). The resulting PEC supported 19 vibrational levels, i.e., five levels more than what was observed experimentally (17). Four decades later, in an effort to characterize states with v'' > 13, Knöckel et al. examined the $A^1\Sigma_u^+ \to X^1\Sigma_g^+$ transition using laser-induced fluorescence (LIF) (20, 21), repeating and refining the earlier LIF experiment by Scheingraber and Vidal (22). They improved and expanded the original ²⁴Mg₂ data set of Balfour and Douglas by reporting a total of 333 G(v'', J'') and 1351 G(v', J'')J') rovibrational term values involving v'' = 0-13 and v' = 1-46, respectively, and constructed a few experimentally derived analytical forms of the $X^1\Sigma_g^+$ PEC, extrapolated to the asymptotic region using the theoretical C₆ (23), C₈ (24), and C₁₀ (24) coefficients, which support the discrete spectral data in the 3.27-8.33 Å range (20). Although these refined PECs supported 19 ²⁴Mg₂ vibrational levels, reinforcing the initial prediction of Li and Stwalley (17), Knöckel et al. were unable to identify $A^1\Sigma_u^+(v', J') \to X^1\Sigma_g^+(v'', J'')$ transitions involving the elusive high-lying vibrational levels with v'' > 13 in their LIF spectra (20).

Typically, high-lying vibrational states near dissociation constitute a small fraction of the entire vibrational manifold, but this is not the case for the weakly bound magnesium dimer, which has a shallow minimum on the ground-state PEC at $r_e = 3.89039$ Å (20) and a tiny dissociation energy D_e of 430.472(500) cm⁻¹ (20, 21). If the five extra levels, which have been speculated about, truly existed, they would represent more than a quarter of the entire vibrational manifold in the ground electronic state. Furthermore, without precise knowledge of the ground-state PEC of Mg₂, especially its long-range part which determines the positions of the high-lying vibrational states near the dissociation threshold, one cannot accurately interpret the aforementioned ultracold and collisional phenomena involving interacting magnesium atoms. It is intriguing why a



10

15

20

25

30

35

40

seemingly docile main group diatomic continues to challenge state-of-the-art spectroscopic techniques. The experimental difficulties in detecting the elusive v'' > 13 states of the magnesium dimer originate from several factors, including small energy gaps between high-lying vibrations that are comparable to rotational spacings (12, 25), resulting in overlapping spectral lines, and unfavorable signal-to-noise ratio in the existing LIF spectra (20). Rotational effects complicate the situation even more, since, in addition to affecting line intensities (20, 22, 25), they may render the high-lying vibrational states of Mg2 unbound. All of these and similar difficulties prompted Knöckel *et al.* to conclude that experimental work alone is insufficient and that accurate theoretical calculations are needed to guide further analysis of the ground-state PEC and rovibrational states of Mg2, especially the elusive v'' > 13 levels near the dissociation threshold (20, 21).

Unfortunately, there have only been a handful of theoretical investigations attempting to determine the entire vibrational manifold of the magnesium dimer. This is, in significant part, related to the intrinsic complexity of the underlying electronic structure and difficulties with obtaining an accurate representation of the ground-state PEC using purely *ab initio* quantum-chemical means. At the Hartree–Fock theory level, which neglects electron correlation and dispersion interactions, Mg₂ remains unbound. As demonstrated in this work, one needs to go to much higher theory levels, incorporate high-order many-electron correlation effects, including valence as well as inner-shell electrons, and employ large, carefully calibrated, one-electron basis sets to accurately capture the relevant physics and obtain a reliable description of the $X^1\Sigma_g^+$ potential and of the corresponding rovibrational manifold (see (26) for a detailed discussion and historical account, including references to the earlier quantum chemistry computations for the magnesium dimer). *Ab initio* quantum mechanical calculations for the $A^1\Sigma_u^+$ PEC, the rovibrational states supported by it, and the $X^1\Sigma_g^+ - A^1\Sigma_u^+$ electronic transition dipole moment function, needed to interpret and aid the photoabsorption and LIF experiments using purely theoretical means, are similarly challenging, and the present study shows this too.

The initial theoretical estimates of the number of vibrational states supported by the $X^l\Sigma_g^+$ potential ranged from 18 to 20 (27), while the more recent ab initio quantum chemistry computations based on the various levels of coupled-cluster (CC) theory (28), reported in (26, 29), suggested that the highest vibrational level of ${}^{24}\text{Mg}_2$ is v'' = 18. Among the previous theoretical studies, only Amaran et al. (29) considered the $A^{1}\Sigma_{1}^{+}$ state involved in the photoabsorption and LIF experiments and included rotational effects, but they have not provided any information about the calculated rovibrational term values other than the root-mean-square deviations (RMSDs) relative to the experimental data of Balfour and Douglas (12). Furthermore, as demonstrated in our recent benchmark study (26), where a large number of CC methods were tested using the $X^1\Sigma_g^+$ PEC of the magnesium dimer and the rotationless term values of ²⁴Mg₂ as examples, and consistent with the earlier calculations (30, 31), the popular CCSD(T) approximation (32) exploited in (29) could not possibly produce the small RMSD value reported in (29), of 1.3 cm⁻¹, for the rovibrational manifold of Mg₂ in its ground electronic state; the value on the order of a dozen cm⁻¹ would be more appropriate (26) (see Fig. S1 in the Supplementary Materials to this work (33)). Similar remarks apply to the $A^1\Sigma_n^+$ state, which was treated in (29) using the low-level variant of the linearresponse CC theory (34), resulting in noticeable deviations from the experimentally derived $A^{1}\Sigma_{n}^{+}$ potential shown in Fig. 4 of (21). To simulate and properly interpret the $A^1\Sigma_u^+ \to X^1\Sigma_g^+$ LIF spectra obtained in (20) using purely theoretical means, one needs much higher accuracy levels in the



10

15

20

25

30

35

40

computations of line positions and robust information about line intensities, which has not been obtained in the previous quantum chemistry studies.

The call for a reliable ab initio computation of the ground-state PEC and rovibrational states of Mg₂, including the v'' > 13 levels that have eluded experimentalists for decades, expressed by Knöckel et al. in (20, 21), is answered in the present work. We report the highly accurate PECs for the ground, $X^1\Sigma_g^+$, and excited, $A^1\Sigma_g^+$, electronic states, involved in the previous experimental investigations of Mg2 (12, 20-22), obtained with state-of-the-art ab initio quantum chemistry, and use them to determine the corresponding rovibrational manifolds. Consistent with the conclusions of our recent benchmark study (26), to obtain a highly accurate representation of the ground-state PEC, we combine the numerically exact description of the valence electron correlation effects, provided by the full configuration interaction (CI) approach, with the nearly exact description of subvalence correlations involving all electrons but the 1s shells of Mg atoms offered by the CC theory with a full treatment of singly, doubly, and triply excited clusters, abbreviated as CCSDT (35, 36). Our computational protocol for the $A^{1}\Sigma_{n}^{+}$ excited state, which we did not consider in (26), is similar, except that in order to capture subvalence electron correlation effects in this state we adopt one of the carefully chosen approximations to the equation-of-motion (EOM) CC theory (37) with singles, doubles, and triples (EOMCCSDT) (38, 39) belonging to the completely renormalized CR-EOMCCSD(T) family (40), which is considerably more affordable than EOMCCSDT without significant loss of accuracy. As in the case of the $X^1\Sigma_g^+$ state, the remaining electron correlations originating from the valence shells are captured using full CI. Based on examining basis set effects (see (33) for details), in order to obtain reasonably well converged rovibrational and LIF spectra, needed to correctly interpret the available experimental or experimentally derived data (12, 17, 20, 21), and accurately describe the relevant many-electron correlation effects, the electronic structure calculations reported in this work rely on the carefully calibrated augmented polarized valence and weighted core-valence correlation-consistent bases of quadruple- ζ quality developed in (41), designated as aug-cc-pV(Q+d)Z and aug-cc-pwCVQZ, respectively. We used these basis sets in our earlier benchmark calculations for the ground state of the magnesium dimer (26), but only for the methods up to CCSDT, i.e., the important post-CCSDT electron correlation effects were treated in (26) with smaller, less saturated, bases.

In order to make our comparisons with experiment more complete, for each of the two electronic potentials considered in this study, we examine both the most abundant 24 Mg₂ species and the 24 Mg 25 Mg, 24 Mg 26 Mg, 25 Mg₂, 25 Mg 26 Mg, and 26 Mg₂ isotopologs (to our knowledge, rovibrational levels of the Mg₂ species other than 24 Mg₂ have not been calculated using *ab initio* potentials before). We combine the above information with the $X^1\Sigma_g^+ - A^1\Sigma_u^+$ electronic transition dipole moment function resulting from the same valence full CI computations as used in the PEC determination to accurately simulate the LIF spectra reported in (20, 21), including line positions and the corresponding line intensities, as defined via the Einstein coefficients, and provide the long-awaited theoretical guidance for the possible experimental detection of the $A^1\Sigma_u^+(v^i, J^i) \rightarrow X^1\Sigma_g^+(v^u, J^u)$ rovibronic transitions involving the $v^u > 13$ levels.

RESULTS

The most essential numerical information, generated in the present study using the computational protocol described in the Materials and Methods section, is summarized in Figs. 1–



3 and Tables 1–3. All of the numerical data supporting the content and conclusions of this work are included in the main text and compiled in the Supplementary Materials document and the Data S1 and S2 archives attached to it (33). In describing and discussing our results, we begin with the PECs and rovibrational term values characterizing the $X^1\Sigma_g^+$ and $A^1\Sigma_u^+$ states of the magnesium dimer, focusing on a comparison of our *ab initio* calculations with the available experimental and experimentally derived data reported in (12, 20, 21). Next, we compare the experimental LIF spectra reported in (20, 21) with those resulting from our computations, and suggest potential avenues for detection of the elusive v'' > 13 levels of the magnesium dimer. Auxiliary information, which complements the discussion in this section, including further comments on the accuracy and convergence characteristics of the computational protocol employed in the present study, the effect of isotopic substitution on the calculated rovibrational term values, the discussion of the validity of the Franck–Condon analysis adopted in (20) to examine the LIF spectra reported in (20, 21), and the lifetimes for predissociation by rotation characterizing quasi-bound rovibrational states supported by the $X^1\Sigma_g^+$ potential, is provided in (33).

Potential energy curves and rovibrational states

As shown in Table 1, our *ab initio* $X^1\Sigma_g^+$ PEC reproduces the experimentally derived dissociation energy D_e and equilibrium bond length r_e of Mg2 (20, 21) to within 0.9 cm⁻¹ (0.2 %) and 0.003 Å (0.07 %), respectively. These high accuracies in describing D_e and r_e are reflected in our calculated rovibrational term values of 24 Mg2 and its isotopologs, which are in very good agreement with the available experimental information (12, 20, 21). As shown in the spreadsheets included in the Data S1 archive in (33), the RMSDs characterizing our *ab initio* $G(v^u, J^u)$ values for 24 Mg2 relative to their experimentally determined counterparts, reported in (12) for $v^u < 13$ and (20, 21) for $v^u < 14$, are 1.1 cm⁻¹, when the spectroscopic data from (12) are used, and 1.5 cm⁻¹, when we rely on (20, 21) instead. At the same time, the maximum unsigned errors in our calculated $G(v^u, J^u)$ values relative to experiment do not exceed ~2 cm⁻¹, even when the quasi-bound states above the potential asymptote arising from centrifugal barriers are considered. Although the experimental information about the $G(v^u, J^u)$ values characterizing other Mg2 isotopologs is limited to 24 Mg 25 Mg, 24 Mg 26 Mg, and 26 Mg2 and includes very few v^u values (20, 21), the RMSDs relative to experiment resulting from our calculations are similarly small (1.0 cm⁻¹ for 24 Mg 25 Mg, 1.2 cm⁻¹ for 24 Mg 26 Mg, and 0.6 cm⁻¹ for 26 Mg2; cf. (33)).

Further insights into the quality of our *ab initio* calculations for the ground-state PEC can be obtained by comparing the resulting rovibrational term values with their counterparts determined using the most accurate, experimentally derived, analytical forms of the $X^1\Sigma_g^+$ potential to date constructed in (20). In the discussion below, we focus on the so-called X-representation of the ground-state PEC developed in (20), which the authors of (20) regard as a reference potential in their analyses (see Table 2). We recall that the X-representation of the ground-state PEC of the magnesium dimer was obtained by simultaneously fitting the $X^1\Sigma_g^+$ and $A^1\Sigma_u^+$ PECs to a large number of the experimentally determined $A^1\Sigma_u^+$ (ν' , J') $\rightarrow X^1\Sigma_g^+$ (ν'' , J'') rovibronic transition frequencies and extrapolating the resulting $X^1\Sigma_g^+$ PEC to the asymptotic region using the theoretical C_6 (23), C_8 (24), and C_{10} (24) coefficients. As shown in Table 2, our *ab initio* $G(\nu'', J'')$ energies characterizing the most abundant $^{24}Mg_2$ isotopolog are in very good agreement with those generated using the X-representation of the ground-state PEC developed in (20). When all of the



10

15

20

25

30

35

40

45

rovibrational bound states supported by both potentials are considered, the RMSD and the maximum unsigned error characterizing our *ab initio* G(v'', J'') values for $^{24}\text{Mg}_2$ relative to their counterparts arising from the X-representation are 1.3 and 2.0 cm⁻¹, respectively. What is especially important in the context of the present study, our *ab initio* ground-state PEC and the state-of-the-art analytical fit to the experimental data defining the X-representation, constructed in (20), bind the v'' = 18 level if the rotational quantum number J'' is not too high (see the discussion below).

The high quality of our calculated G(v'', J'') values and spacings between them, which can also be seen in Tables 1 and 2 and Fig. 1, allows us to comment on the existence of the v'' > 13levels that have escaped experimental detection for decades. As already alluded to above and as shown in Table 2 and Fig. 1, our ab initio $X^{1}\Sigma_{g}^{+}$ PEC supports the same number of rotationless vibrational levels as the latest experimentally derived PEC defining the X-representation (20), which for the most abundant ²⁴Mg₂ isotopolog is 19 (see (33) for the information about the remaining Mg₂ species). Table 1, which compares the rovibrational term values of ²⁴Mg₂ resulting from our *ab initio* calculations for the representative rotational quantum numbers ranging from 0 to 80 with the available experimental data, shows that the elusive high-lying states with v'' > 13quickly become unbound as J" increases, so by the time J'' = 20, the v'' = 15-18 levels are no longer bound (see Fig. S3 for a graphical representation of the J'' = 20, 40, 60, and 80 effective potentials including centrifugal barriers characterizing the rotating ²⁴Mg₂ molecule, along with the corresponding vibrational wave functions and information about the lifetimes for predissociation by rotation associated with tunneling through centrifugal barriers characterizing quasi-bound states). In fact, according to our ab initio data compiled in (33), the maximum rotational quantum number that allows for at least one bound rovibrational state decreases with v'', from J'' = 68 for v'' = 0 to J'' = 4 for v'' = 18, with all states becoming quasi-bound or unbound when $J'' \ge 70$, when the most abundant ²⁴Mg₂ isotopolog is considered. In general, as shown in Fig. S3 and the lifetime data compiled in (33), the mean lifetimes for predissociation by rotation characterizing quasibound states with a given J" rapidly decrease as v" becomes larger. They decrease equally fast when J'' increases and v'' is fixed. These observations imply that the spectroscopic detection of the high-lying vibrational states of Mg₂ can only be achieved if the molecule does not rotate too fast (cf. Table 1 and Fig. S3). We could not find any information regarding the timescales involved in the LIF experiments carried out by Knöckel et al. (20). However, a comparison of our ab initio determined quasi-bound rovibrational states, including their energies and lifetimes compiled in (33), with the observed rovibronic transitions reported in the Supplementary Material to (21) suggests that the mean lifetimes for predissociation by rotation characterizing quasi-bound states seen in the experimentally resolved LIF spectral lines are on the order of 0.1 ns or longer.

As shown in Fig. 1, where we plot the wave functions of the high-lying, purely vibrational, states of $^{24}\text{Mg}_2$, starting with the last experimentally observed v'' = 13 level, along with the $X^1\Sigma_g^+$ PEC obtained in our *ab initio* calculations, the v'' = 18 state, located only 0.2 cm⁻¹ below the potential asymptote, is barely bound (see, also, Table 1). This makes the existence of an additional, v'' = 19, level for the most abundant isotopolog of the magnesium dimer unlikely. Further insights into the number of purely vibrational bound states of $^{24}\text{Mg}_2$ supported by the $X^1\Sigma_g^+$ PEC are provided by the inset in Fig. 1, where we plot the rotationless G(v'' + 1) - G(v'') energy differences, resulting from the *ab initio* calculations reported in this work and experiment, as a function of $v'' + \frac{1}{2}$ (the Birge–Sponer plot). Fitting the experimental data to a line, *i.e.*, assuming a Morse potential, results in v'' = 16 being the last bound vibrational level of $^{24}\text{Mg}_2$. Although the deviation



10

15

20

25

30

35

40

from the Morse potential, as predicted by our *ab initio* calculations, is not as severe as in the case of Be₂ (11), it is significant enough to result in the v'' = 17 and 18 states becoming bound, emphasizing the importance of properly describing the long-range part of the PEC.

As shown in Table 1 and Fig. 1, the G(v'' + 1) - G(v'') vibrational spacings rapidly decrease with increasing v", from 47.7 cm⁻¹ or 68.6 K for v" = 0 to 11.7 cm⁻¹ or 16.8 K for v" = 12, and to 0.8 cm^{-1} or 1.2 K for v'' = 17, when $^{24}\text{Mg}_2$ is considered. This means that at regular temperatures all vibrational levels of the magnesium dimer, which is a very weakly bound system, are significantly populated, making selective probing of the closely spaced higher-energy states, including those with v'' > 13, virtually impossible, since practically every molecular collision (e.g., with another dimer) may result in a superposition of many rovibrational states, with some breaking the dimer apart. At room temperature, for example, the cumulative population of the v'' > 13 states of ²⁴Mg₂, determined using the normalized Boltzmann distribution involving all rotationless levels bound by the $X^1\Sigma_{\sigma}^+$ potential, of about 12 %, is comparable to the populations of the corresponding low-lying states (16 % for v'' = 0, 13 % for v'' = 1, and 10 % for v'' = 2). The situation changes in the cold/ultracold regime, where the available thermal energies, which are on the order of mK or even μK , are much smaller than the vibrational spacings, even when the high-lying states with ν " > 13 near the dissociation threshold are considered, suppressing collisional effects and allowing one to probe the long-range part of the ground-state PEC, where the v'' > 13 states largely localize (cf. Fig. 1). This makes the accurate characterization of the v'' > 13 bound and quasi-bound states provided by the high-level ab initio calculations reported in this work relevant to the applications involving cold/ultracold Mg atoms separated by larger distances in magneto-optical traps (see, e.g., (6)).

The accuracy of our *ab initio* description of the more strongly bound $A^1\Sigma_n^+$ electronic state $(D_e = 9414 \text{ cm}^{-1} \text{ and } r_e = 3.0825 \text{ Å} (21); \text{ cf. Fig. 2 for the corresponding PEC}), which we need to$ consider in order to simulate the LIF spectra, is consistent with that obtained for the weakly bound ground state. For example, the errors relative to experiment (21) resulting from our calculations of the dissociation energy D_e and equilibrium bond length r_e are 0.91 % (86 cm⁻¹) and 0.2 % (0.006 Å), respectively (see (33)). This high accuracy of our ab initio $A^{1}\Sigma_{u}^{+}$ PEC is reflected in the excellent agreement between the $^{24}Mg_2$ G(v', J') values obtained in this work and their experimentally derived counterparts reported in (12, 21). In particular, the RMSDs characterizing our rovibrational term values in the $A^{1}\Sigma_{n}^{+}$ state relative to the data of Balfour and Douglas (12) and Knöckel et al. (21) are only 3.2 and 4.5 cm⁻¹, respectively, which is a major improvement over the RMSD of 30 cm⁻¹ reported in (29). They are similarly small for the rovibrational states supported by the $A^1\Sigma_n^+$ potential that characterize the remaining, experimentally observed, $^{24}Mg^{25}Mg$, 24 Mg 26 Mg, and 26 Mg₂ isotopologs examined in (21) (3.7, 4.1, and 4.1 cm $^{-1}$, respectively; *cf.* (33)). According to our *ab initio* calculations using the computational protocol described in the Materials and Methods section, the total number of vibrational states supported by the $A^{1}\Sigma_{n}^{+}$ potential well for the most abundant ²⁴Mg₂ species is 169 (see the Data S1 archive in (33)).

Laser-induced fluorescence: Ab initio theory vs experiment

The most compelling evidence for the predictive power of our *ab initio* electronic structure and rovibrational calculations is the nearly perfect reproduction of the experimental $A^1\Sigma_u^+ \to X^1\Sigma_g^+$ LIF spectrum reported in (20, 21), shown in Fig. 3 and Table 3, with further information provided



in (33). Figure 2 uses our calculated $X^1\Sigma_g^+$ and $A^1\Sigma_u^+$ PECs and the corresponding rovibrational wave functions to illustrate the photoexcitation and fluorescence processes that resulted in the experimental LIF spectrum shown in Fig. 3 of (20), which is reproduced in Fig. 3A. This particular spectrum represents the fluorescence progression from the $A^1\Sigma_u^+(v'=3,J'=11)$ state of $^{24}\text{Mg}_2$, populated by laser excitation from the $X^1\Sigma_g^+(v''=5,J''=10)$ state, to all accessible $X^1\Sigma_g^+(v'',J'')$ rovibrational levels, resulting in the P12/R10 doublets that correspond to J''=12 for the P branch and J''=10 for the R branch. Figure 3 and Table 3 compare the experimentally observed $A^1\Sigma_u^+(v'=3,J'=11)\to X^1\Sigma_g^+(v'',J''=10,12)$ transitions with the corresponding line positions (Fig. 3 and Table 3) and intensities (Fig. 3) resulting from our *ab initio* calculations. The only adjustment that we made to produce the theoretical LIF spectrum shown in Fig. 3 and Table 3 was a uniform shift of the entire $A^1\Sigma_u^+$ PEC obtained in our *ab initio* computations in order to match the experimentally determined adiabatic electronic excitation energy T_e of 26068.9 cm⁻¹ (21) (see the Materials and Methods section for the details). Other than that, the theoretical LIF spectrum in Fig. 3 and Table 3 relies on the raw *ab initio* electronic structure and rovibrational data.

The striking agreement between the theoretical and experimental LIF spectra shown in Fig. 3A and Table 3, with differences in line positions not exceeding 1–1.5 cm⁻¹ and with virtually identical intensity patterns, suggests that our predicted transition frequencies involving the elusive v'' > 13 states are very accurate, allowing us to provide guidance for their potential experimental detection in the future. Before discussing our suggestions in this regard, we note that thanks to our *ab initio* calculations, we can now locate the previously unidentified P12/R10 doublets involving the v'' > 13 states within the experimental LIF spectrum reported in Fig. 3 of (20). Indeed, as shown in Fig. 3 and Table 3, the LIF spectrum corresponding to the $A^1\Sigma_u^+(v'=3,J'=11) \to X^1\Sigma_g^+(v'',J'') = 10,12$) transitions contains the P12/R10 doublets involving the v'' = 0-16 states and the R10 line involving the v'' = 17 state. The $A^1\Sigma_u^+(v'=3,J'=11) \to X^1\Sigma_g^+(v''=17,J''=12)$ and $A^1\Sigma_u^+(v'=3,J'=11) \to X^1\Sigma_g^+(v''=17,J''=12)$ and $A^1\Sigma_u^+(v'=3,J''=10) \to X^1\Sigma_g^+(v''=17,J''=12)$ and $A^1\Sigma_u^+(v'=17,J''=12) \to X^1\Sigma_g^+(v''=12)$ and $A^1\Sigma_u^+(v'=12) \to X^1\Sigma_g^$

As one can see by inspecting the Data S2 archive in (33) and Fig. 3, and consistent with the remarks made by Knöckel *et al.* in (20), the experimental detection of the P12/R10 doublets involving v'' > 13, when transitioning from the $A^1\Sigma_u^+(v'=3, J'=11)$ state, was hindered by the unfavorable signal-to-noise ratio (transitions to the v''=16 and 17 states exhibit low Einstein coefficients) and the presence of overlapping lines outside the P12/R10 progression, originating from collisional relaxation effects (20) and having similar (v''=15) or higher (v''=14) intensities. In order to fully appreciate this, in Fig. 3B we magnified the region of the LIF spectrum recorded in (20) that contains the calculated $A^1\Sigma_u^+(v'=3, J'=11) \to X^1\Sigma_g^+(v''=13-16, J''=10,12)$ and $A^1\Sigma_u^+(v'=3, J'=11) \to X^1\Sigma_g^+(v''=17, J''=10)$ transitions. As shown in Fig. 3 and Table 3, the identification of the P12/R10 doublets corresponding to the $A^1\Sigma_u^+(v'=3, J'=11) \to X^1\Sigma_g^+(v''=0-13, J''=10,12)$ transitions is unambiguous. The observed and calculated line positions and intensities and line intensity ratios within every doublet match each other very closely. Figure 3B demonstrates that the identification of the remaining doublets in the P12/R10 progression is much harder. Based on our *ab initio* work and taking into account the fact that our calculated line



10

15

20

25

30

35

40

positions may be off by about 1 cm⁻¹ (*cf.* Table 3), the v'' = 14 P12/R10 doublet, marked in Fig. 3B by the blue arrows originating from the v'' = 14 label, is largely hidden behind the higher-intensity feature that does not belong to the P12/R10 progression and that most likely originates from collisional relaxation (*20*). Thanks to our calculations, we can also point to the most likely location of the v'' = 15 P12/R10 doublet in the LIF spectrum recorded in (*20*) (see the blue arrows originating from the v'' = 15 label in Fig. 3B). Doing this without backing from theory is virtually impossible due to the presence of other lines near the $A^1\Sigma_u^+(v'=3, J'=11) \to X^1\Sigma_g^+(v''=15, J''=10,12)$ transitions having similar intensities. As shown in Fig. 3B, the situation with the remaining $A^1\Sigma_u^+(v'=3, J'=11) \to X^1\Sigma_g^+(v''=16, J''=10,12)$ and $A^1\Sigma_u^+(v'=3, J'=11) \to X^1\Sigma_g^+(v''=17, J''=10)$ transitions is even worse, since they have very low Einstein coefficients that hide them in the noise.

Knöckel et al. also suggested that the difficulties with detecting the P12/R10 doublets involving the v'' = 14 and 15 states, which have higher Franck-Condon factors than those characterizing the experimentally observed $A^1\Sigma_u^+(v'=3, J'=11) \to X^1\Sigma_g^+(v''=0, J''=10,12)$ transitions, might be related to the variation of the $X^1\Sigma_g^+ - A^1\Sigma_u^+$ electronic transition dipole moment function $\mu_z^{(X-A)}(r)$ with the internuclear separation r and limitations of the Franck-Condon principle (20), but our ab initio calculations do not confirm this. As shown in (33) (see Fig. S2), in the region of r values where the respective rovibrational wave functions, $\chi_{v'',J''}^{(X)}(r)$, with v'' = 14, 15 and J'' = 10, 12 for the $X^{1}\Sigma_{g}^{+}$ state, and $\chi_{v',J'}^{(A)}(r)$, with v' = 3 and J' = 11 for the $A^{1}\Sigma_{u}^{+}$ state, overlap, changes in $\mu_{z}^{(X-A)}(r)$ do not exceed 3 %, i.e., the Frank-Condon analysis is well justified. Furthermore, $\mu_z^{(X-A)}(r)$ does not vary too much, even when the entire r = 2.2-100.0Å region examined in this work is considered. In agreement with the analysis presented in (20), our calculated Franck-Condon factors for the v'' = 14 and 15 P12/R10 doublets are indeed higher than those characterizing the analogous v'' = 0 lines, but, as demonstrated in the Data S2 archive in (33), the same holds for the respective Einstein coefficients. Thus, it is the presence of densely spaced and overlapping lines outside the P12/R10 progression having similar or higher intensities than the $A^1\Sigma_u^+$ (v'=3, J'=11) $\to X^1\Sigma_g^+$ (v''=14,15, J''=10,12) transitions that makes the experimental identification of the v'' = 14 and 15 P12/R10 doublets very hard.

Theory-inspired avenues for detection of elusive states

In general, our *ab initio* calculations carried out in this work indicate that under the constraints of the LIF experiments reported in (20, 21), where the authors populated the $A^1\Sigma_u^+(v', J')$ states with v' = 1–46, the $X^1\Sigma_g^+(v'', J'')$ states with v'' = 14–18 cannot be realistically detected due to very small Franck–Condon factors and Einstein coefficients characterizing the corresponding $A^1\Sigma_u^+(v', J') \to X^1\Sigma_g^+(v'', J'')$ transitions (see the Data S2 archive in (33)). As shown in Fig. 1, the v'' = 14–18 states are predominantly localized in the long-range r = 8–16 Å region. At the same time, as illustrated in Fig. 2, the potential well characterizing the electronically excited $A^1\Sigma_u^+$ state is much deeper and shifted toward shorter internuclear separations compared to its $X^1\Sigma_g^+$ counterpart. Thus, the only way to access the $X^1\Sigma_g^+(v'', J'')$ states with v'' = 14–18 via fluorescence from $A^1\Sigma_u^+$ is by populating the high-lying $A^1\Sigma_u^+(v', J')$ levels with $v' \gg 46$.



10

15

20

25

30

35

40

In an effort to assist the experimental community in detecting the elusive v'' = 14-18vibrational levels, we searched for the $A^1\Sigma_n^+(v',J') \to X^1\Sigma_n^+(v''=14-18,J''=J'\pm 1)$ transitions in the most abundant isotopolog of the magnesium dimer, ²⁴Mg₂, that would result in spectral lines of maximum intensity based on the Einstein coefficients compiled in the Data S2 archive in (33). To ensure the occurrence of allowed transitions involving the last, v'' = 18, level, which for ²⁴Mg₂ becomes unbound when J'' > 4, we focused on the J'' values not exceeding 4, i.e., the fluorescence from the $A^{1}\Sigma_{n}^{+}(v', J')$ states with J' = 1, 3, and 5. According to our calculations, the optimum v'values for observing the v'' = 14-18, $J'' \le 4$ states via the LIF spectroscopy are in the neighborhood of v' = 60, 66–69, and 74–84 for v'' = 14; 72–75 and 80–91 for v'' = 15; 79–82 and 88–100 for v''= 16; 88, 89, and 97–111 for v'' = 17; and 109–129 for v'' = 18 (see the Data S2 archive in (33) for the details of all allowed rovibronic transitions in $^{24}\text{Mg}_2$ involving the $X^1\Sigma_g^+$ and $A^1\Sigma_u^+$ states, including, in particular, the relevant $X^{l}\Sigma_{g}^{+}(v'',J''\leq 4) \rightarrow A^{l}\Sigma_{u}^{+}(v',J')$ pump and $A^{l}\Sigma_{u}^{+}(v',J''=1,3,5)$ $\to X^1\Sigma_q^+(v''=14-18, J''\leq 4)$ fluorescence processes). In determining these optimum v' values, we chose the cutoff of 1.0×10⁷ Hz in the Einstein coefficients, which is similar to the Einstein coefficients calculated for the most intense v'' = 5 P12/R10 doublet in the experimental LIF spectrum shown in Fig. 3 of (20), reproduced in Fig. 3A. Our predicted $A^{1}\Sigma_{n}^{+}(v', J'=1,3,5) \rightarrow X^{1}\Sigma_{n}^{+}$ (v'' = 14-18, $J'' \le 4$) fluorescence frequencies resulting from the aforementioned optimum v'ranges, which might allow one to detect the v'' = 14-18 states of $^{24}\text{Mg}_2$ via a suitably designed LIF experiment, are estimated at about 33360, 33740–33910, and 34150–34530 cm⁻¹ for v'' = 14; 34050-34190 and 34390-34710 cm⁻¹ for v'' = 15; 34350-34460 and 34640-34880 cm⁻¹ for v'' = 1516; 34630–34660 and 34830–35000 cm⁻¹ for v'' = 17; and 34990–35100 cm⁻¹ for v'' = 18 (given the 86 cm⁻¹ error in the calculated D_e characterizing the $A^{\rm I}\Sigma_{\rm u}^{+}$ state and the RMSD of ~3–5 cm⁻¹ in our $^{24}\text{Mg}_2$ G(v', J') values relative to the spectroscopic data of (12, 21), the above frequency ranges may have to be shifted by a dozen or so cm⁻¹).

DISCUSSION

We used state-of-the-art *ab initio* quantum-mechanical methodologies to address a half-century-old enigma regarding the v''=14–18 vibrational states of the magnesium dimer. We provided the highly accurate ground-state PEC and rovibrational term values of ²⁴Mg₂ and its less abundant ²⁴Mg²⁵Mg, ²⁴Mg²⁶Mg, ²⁵Mg₂, ²⁵Mg²⁶Mg, and ²⁶Mg₂ isotopologs. We demonstrated that the $X^1\Sigma_g^+$ PEC supports rovibrational levels of ²⁴Mg₂ up to v''=18, although the elusive v''>13 states become unbound as the rotational quantum number J'' increases, which contributes to difficulties with their experimental detection. We also obtained an accurate representation of the $A^1\Sigma_u^+$ potential, which, according to our calculations, supports 169 vibrational states of ²⁴Mg₂, and, with the help of the *ab initio* electronic transition dipole moment function, determined in this study as well, accurately simulated the LIF spectra recorded in (20, 21), including line positions and intensities. Our work provides the long-awaited guidance for possible experimental identification of rovibronic transitions involving the v''>13 levels that have eluded scientists for five decades.

We hope that this study will fuel new spectroscopic investigations of the challenging Mg₂ species and its heavier Group 2 analogs, which are important in a variety of phenomena at the intersection of chemistry and atomic, molecular, and optical physics. A few years ago, *ab initio* calculations (8) combined with spectroscopic analyses (7, 10) led to the discovery of the elusive twelfth vibrational level of the beryllium dimer. By dealing with five similarly challenging states



10

15

20

25

30

35

40

in a system three times larger than Be₂, we demonstrated that the predictive power of modern *ab initio* quantum chemistry is no longer limited to small few-electron species.

MATERIALS AND METHODS

Ab initio electronic structure calculations

The goal of the *ab initio* electronic structure calculations performed in this study was to obtain highly accurate $X^1\Sigma_g^+$ and $A^1\Sigma_u^+$ PECs of the magnesium dimer and the corresponding $X^1\Sigma_g^+ - A^1\Sigma_u^+$ transition dipole moment function $\mu_z^{(X-A)}(r)$ involved in the photoabsorption and LIF experiments reported in (12, 20–22). In the case of the ground-state PEC, we combined the numerically exact description of the valence electron correlation effects provided by full CI with the high-level description of subvalence correlations involving all electrons but the 1s shells of Mg atoms obtained using CCSDT (35, 36). Thus, the $X^1\Sigma_g^+$ PEC of Mg₂ reported in this work was obtained by utilizing the composite scheme

$$E_{\mathbf{X}^{1}\Sigma_{o}^{+}} = E_{\mathbf{X}^{1}\Sigma_{o}^{+}}^{(\text{CCSDT/AwCQZ})} + \left(E_{\mathbf{X}^{1}\Sigma_{o}^{+}}^{(\text{Full CI/A}(\mathbf{Q}+d)\mathbf{Z})} - E_{\mathbf{X}^{1}\Sigma_{o}^{+}}^{(\text{CCSDT/A}(\mathbf{Q}+d)\mathbf{Z})}\right). \tag{1}$$

The first term on the right-hand side of Eq. (1) denotes the total electronic energy obtained in the full CCSDT calculations correlating all electrons other than the 1s shells of the Mg monomers and using the aug-cc-pwCVOZ basis set developed in (41), abbreviated in this section and in (33) as AwCQZ. The second and third terms on the right-hand side of Eq. (1), which represent the difference between the frozen-core full CI and CCSDT energies obtained using the aug-ccpV(Q+d)Z basis of (41), abbreviated in this section and in (33) as A(Q+d)Z, correct the nearly allelectron CCSDT/AwCOZ energy for the valence correlation effects beyond CCSDT. The A(Q+d)Z and AwCQZ basis sets were taken from the Peterson group's website (42). We used these bases rather than their standard aug-cc-pVnZ and aug-cc-pCVnZ counterparts, since it has been demonstrated that the aug-cc-pV(n+d)Z and aug-cc-pwCVnZ basis set families, including A(Q+d)Z and AwCQZ, accelerate the convergence of bond lengths, dissociation energies, and spectroscopic properties of magnesium compounds (26, 41). The aug-cc-pV(T+d)Z, aug-ccpwCVTZ, and aug-cc-pwCV5Z bases (41), abbreviated in this section and in (33) as A(T+d)Z, AwCTZ, and AwC5Z, respectively, and utilized in the auxiliary calculations discussed in Section S1 of (33) to demonstrate the convergence of our computational protocol with respect to the basis set size (see Tables S1 and S2 in (33)), were taken from the Peterson group's website (42) as well.

As shown in Section S1 of the Supplementary Materials (33), the AwCQZ and A(Q+d)Z bases are large and rich enough to provide spectroscopic properties of the magnesium dimer that can be regarded as reasonably well converged with respect to the basis set size, to within \sim 0.1–2 cm⁻¹ for the experimentally observed $v'' \leq 13$ levels and \sim 3–5 cm⁻¹ for the remaining high-lying vibrational states and D_e (see, e.g., Table S2 in (33)). Ideally, one would like to improve these results further by extrapolating, for example, the nearly all-electron CCSDT energetics in Eq. (1), which are responsible for the bulk of the many-electron correlation effects in Mg₂, to the complete basis set (CBS) limit. Unfortunately, a widely used two-point CBS extrapolation (43) based on the subvalence CCSDT/AwCTZ and CCSDT/AwCQZ data, which are the only CCSDT data of this type available to us, to determine the CBS counterpart of the first term on the right-hand side of Eq. (1) would not be reliable enough. As demonstrated in (26) and as elaborated on in Section S1 of (33) (see Table S2), a CBS extrapolation using the AwCTZ and AwCQZ basis sets worsens, instead of improving, the D_e , r_e , and vibrational term values of the magnesium dimer compared to



the unextrapolated results using the AwCQZ basis. As shown in Table S2 of (33), the CBS extrapolation using the AwCQZ and AwC5Z basis sets would be accurate enough, but the CCSDT/AwC5Z calculations for the magnesium dimer correlating all electrons but the 1s shells of Mg atoms are prohibitively expensive. One could try to address this concern by replacing CCSDT in Eq. (1) by the more affordable CCSD(T) approach (32), resulting in

$$\tilde{E}_{\mathbf{X}^{1}\Sigma_{\mathbf{g}}^{+}} = E_{\mathbf{X}^{1}\Sigma_{\mathbf{g}}^{+}}^{(\text{CCSD(T)/AwCQZ})} + \left(E_{\mathbf{X}^{1}\Sigma_{\mathbf{g}}^{+}}^{(\text{Full CI/A(Q+d)Z})} - E_{\mathbf{X}^{1}\Sigma_{\mathbf{g}}^{+}}^{(\text{CCSD(T)/A(Q+d)Z})}\right),\tag{2}$$

but, as explained in Section S2 of (33), the computational protocol defined by Eq. (2) is not sufficiently accurate for the spectroscopic considerations reported in this work due to the inadequate treatment of triples by the baseline CCSD(T) approximation (cf. Fig. S1 in (33)). For all these reasons, we have to rely on Eq. (1), in which we use CCSDT, not CCSD(T), and finite (albeit large and carefully optimized) AwCQZ and A(Q+d)Z basis sets rather than the poor-quality CBS extrapolation from the CCSDT/AwCTZ and CCSDT/AwCQZ information.

In principle, one could extend the above composite scheme, given by Eq. (1), to the electronically excited $A^1\Sigma_u^+$ state by replacing CCSDT in Eq. (1) with its EOMCCSDT counterpart (38, 39), but the nearly all-electron full EOMCCSDT calculations using the large AwCQZ basis set turned out to be prohibitively expensive for us. To address this problem, we resorted to one of the CR-EOMCCSD(T) approximations to EOMCCSDT, namely, CR-EOMCCSD(T),IA (40), which is capable of providing highly accurate excited-state PECs of near-EOMCCSDT quality at the small fraction of the cost. Thus, our composite scheme for the calculations of the $A^1\Sigma_u^+$ PEC was defined as

$$E_{\mathbf{A}^{\mathbf{I}}\Sigma_{\mathbf{u}}^{+}} = E_{\mathbf{A}^{\mathbf{I}}\Sigma_{\mathbf{u}}^{+}}^{(\text{CR-EOMCCSD(T),IA/AwCQZ})} + \left(E_{\mathbf{A}^{\mathbf{I}}\Sigma_{\mathbf{u}}^{+}}^{(\text{Full CI/A}(\mathbf{Q}+d)\mathbf{Z})} - E_{\mathbf{A}^{\mathbf{I}}\Sigma_{\mathbf{u}}^{+}}^{(\text{CR-EOMCCSD(T),IA/A}(\mathbf{Q}+d)\mathbf{Z})}\right), \tag{3}$$

where the first term on the right-hand side of Eq. (3) is the total electronic energy of the $A^1\Sigma_u^+$ state obtained in the CR-EOMCCSD(T),IA/AwCQZ calculations correlating all electrons other than the 1s shells of the Mg monomers and the next two terms correct the nearly all-electron CR-EOMCCSD(T),IA/AwCQZ calculations for the valence correlation effects beyond the CR-EOMCCSD(T),IA level using the difference of the full CI and CR-EOMCCSD(T),IA energies obtained with the A(Q+d)Z basis. Prior to deciding on the use of CR-EOMCCSD(T),IA, we tested other CR-EOMCC schemes (44) by comparing the resulting $A^1\Sigma_u^+$ potentials obtained using Eq. (3) and the corresponding rovibrational term G(v', J') values with the available experimentally derived data reported in (21, 45). Although all of these schemes worked well, the computational protocol defined by Eq. (3), with the CR-EOMCCSD(T),IA approach serving as a baseline method, turned out to produce the smallest maximum unsigned errors and RMSD values relative to experiment.

While the $X^1\Sigma_g^+$ and $A^1\Sigma_u^+$ PECs obtained in this study appear to be accurate enough for reproducing and interpreting the experimental $A^1\Sigma_u^+ \to X^1\Sigma_g^+$ LIF spectra reported in (20, 21), one might wonder if the neglect of the post-Born–Oppenheimer and relativistic effects in our *ab initio* calculations could significantly affect our main conclusions. According to (20, 21), the non-adiabatic Born–Oppenheimer corrections (BOCs) for the $X^1\Sigma_g^+$ and $A^1\Sigma_u^+$ states and the mass-dependent adiabatic BOC for the $X^1\Sigma_g^+$ state are negligible. The adiabatic BOC for the $A^1\Sigma_u^+$ state, as defined in (21), may have to be accounted for, but, based on the numerical data reported in (21), its magnitude is well within the uncertainty of the *ab initio* calculations reported in this work.



10

15

20

25

30

35

40

According to (30), special relativity reduces the dissociation energy D_e characterizing the $X^{1}\Sigma_{g}^{+}$ PEC by 4.3 cm^{-1} , i.e., the relativistic effects change the D_e by about 1 %. However, our preliminary analysis using the modified version of the ab initio protocol adopted in the present work, in which the valence full CI and CCSDT calculations using the A(Q+d)Z basis set and the nearly all-electron CCSDT/AwCQZ computations are replaced by their scalar-relativistic counterparts employing the third-order Douglas-Kroll (DK) Hamiltonian (46, 47) and the triple- ζ aug-cc-pV(T+d)Z-DK and aug-cc-pwCVTZ-DK bases (41), demonstrates that the number of bound vibrational states supported by the relativity-corrected $X^{1}\Sigma_{\sigma}^{+}$ potential is exactly the same as in the case of the analogous non-relativistic calculations using the A(T+d)Z and AwCTZ bases (the small negative differences between the relativity-corrected and nonrelativistic rotationless G(v'') values vary from $< 1 \text{ cm}^{-1}$ or 0.8 % for v'' = 0-2 to ~ 1 % for the highest vibrational states near the corresponding dissociation thresholds). Similar applies to the $A^1\Sigma_n^+$ PEC, where the effect of relativity on the D_e value, estimated using the triple-ζ DK analog of the quadruple-ζ non-relativistic computational protocol adopted in this work, is 0.2 %, but the total number of bound vibrational states supported by the non-relativistic and relativity-corrected potentials remains the same. The ab initio vibrational spectra corresponding to the $X^1\Sigma_g^+$ and $A^1\Sigma_u^+$ electronic states obtained using the triple- ζ DK modification of the non-relativistic protocol employed in the present study also show that the effects of relativity on the rotationless G(v''+1) - G(v'') and G(v'+1) - G(v') energy spacings do not exceed 0.4 cm⁻¹ in the former case and 0.3 cm⁻¹ in the case of the latter energy differences. Thus, while our preliminary findings regarding the small, but non-negligible, effects of relativity need a thorough reexamination using both the larger basis sets, such as aug-cc-pV(Q+d)Z-DK and aug-cc-pwCVQZ-DK, and the various truncations in the DK Hamiltonian expansions, which may influence the calculated spectra too (47), and we will return to these issues in the future work, the $X^{l}\Sigma_{g}^{+}$ and $A^{l}\Sigma_{u}^{+}$ PECs obtained in the present study are sufficiently accurate to interpret and analyze the LIF spectra reported in (20, 21) and to comment on the corresponding rovibrational manifolds, especially for the ground electronic state.

All electronic structure calculations for Mg₂ performed in this study, summarized in Tables S3-S5 in (33), were based on the tightly converged restricted Hartree-Fock (RHF) reference functions (the convergence criterion for the RHF density matrix was set up at 10^{-9}). The valence full CI calculations for the $X^1\Sigma_g^+$ and $A^1\Sigma_u^+$ states were performed using the GAMESS package (48), whereas the valence and subvalence CCSDT computations for the $X^{l}\Sigma_{g}^{+}$ state were carried out with NWChem (49). The valence and subvalence CR-EOMCCSD(T),IA calculations for the $A^{1}\Sigma_{n}^{+}$ state were executed using the RHF-based CR-EOMCCSD(T) routines developed in (40), which take advantage of the underlying ground-state CC codes described in (50) and which are part of GAMESS as well. The GAMESS RHF-based CC routines (50) were also used to perform the CCSD(T) calculations needed to explore the basis set convergence and the viability (or the lack thereof) of the alternative to the CCSDT-based composite scheme given by Eq. (1), defined by Eq. (2) (see Sections S1 and S2 in the Supplementary Materials (33), especially Table S2 and Fig. S1). The convergence thresholds used in the post-RHF steps of the CC and EOMCC computations reported in this work were set up at 10^{-7} for the relevant excitation amplitudes and 10⁻⁷ hartree (0.02 cm⁻¹) for the corresponding electronic energies. The default GAMESS input options that were used to define our full CI calculations guaranteed energy convergence to 10^{-10} hartree.



10

15

20

25

30

35

40

The grid of Mg–Mg separations r, at which the electronic energies of the $X^1\Sigma_g^+$ and $A^1\Sigma_u^+$ states reported in this study (cf. Tables S3 and S4 in (33)) were determined, was as follows: 2.2, 2.3, 2.4, 2.5, 2.6, 2.7, 2.8, 2.9, 3.0, 3.1, 3.2, 3.3, 3.4, 3.6, 3.7, 3.8, 3.9, 4.0, 4.1, 4.2, 4.4, 4.6, 4.8, 5.0, 5.2, 5.4, 5.6, 5.8, 6.0, 6.4, 6.8, 7.2, 7.6, 8.0, 8.4, 8.8, 9.2, 9.6, 10.0, 11.0, 12.0, 13.0, 15.0, 20.0, 25.0, 30.0, and 100.0 Å. We adopted the same set of r values to determine the electronic transition dipole moment function $\mu_z^{(X-A)}(r)$ between the $X^1\Sigma_g^+$ and $A^1\Sigma_u^+$ electronic states, needed to calculate LIF line intensities using the Einstein coefficients. The $\mu_z^{(X-A)}(r)$ calculations reported in this work were performed using the valence full CI approach, as implemented in GAMESS, employing the A(Q+d)Z basis set of (41) (see Fig. S2 and Table S5 in (33)).

It is worth pointing out that our *ab initio* data points representing the $X^1\Sigma_g^+$ PEC calculated on the above grid of r values are consistent with the expected long-range physics. One can see this, for example, by comparing our *ab initio* electronic energies for the $X^1\Sigma_g^+$ state compiled in the last column of Table S3 in (33) with their X-representation counterparts obtained using the potential parameters provided in Table I of (20). Indeed, if we align the X-representation and our *ab initio* potentials such that the energies at r = 100.0 Å are identical (without this alignment, the X-representation and our *ab initio* energies at r = 100.0 Å calculated relative to the corresponding potential minima differ by 0.9 cm^{-1}), the differences between the two PECs in the r > 8.5 Å region, where the X-representation potential has the form $V(r) = D_e - \sum_{m=0}^3 C_{6+2m} / r^{6+2m}$, do not exceed 0.8 cm^{-1} , rapidly approaching zero as r increases (r = 100.0 Å is large enough to define the asymptotic region; for example, the difference between the X-representation energies at r = 30.0 Å and r = 100.0 Å is only 0.004 cm^{-1} ; our *ab initio* calculations at the same two r values produce the numerically identical energy difference). In the $r \ge 20$ Å region, where the X-representation energies are flat to within about 0.05 cm^{-1} , the X-representation and shifted *ab initio* energies, as described above, differ by less than 0.01 cm^{-1} .

Calculations of rovibrational term values and rovibronic transitions

The rovibrational term values, including bound and quasi-bound states supported by our ab initio $X^{l}\Sigma_{g}^{+}$ and $A^{l}\Sigma_{u}^{+}$ PECs defined by Eqs. (1) and (3), were computed by numerically integrating the radial Schrödinger equation from 2.2 to 100.0 Å using the Numerov-Cooley algorithm (51) available in the LEVEL16 code (52) (LEVEL16 uses the Airy-function approach described in (53) to locate quasi-bound states). The widths and the tunneling lifetimes for predissociation by rotation characterizing the quasi-bound rovibrational states supported by the $X^{1}\Sigma_{\sigma}^{+}$ potential were calculated using LEVEL16 as well. In this case, we followed the semiclassical procedure described in (52) and implemented in LEVEL16, which requires numerical integrations between turning points in the classically allowed and classically forbidden regions of the relevant effective potentials including centrifugal barriers shown, for example, in Fig. S3 (see (52) for further details). In order to produce electronic energies V(r) on a dense grid of internuclear distances r with the step size of 0.001 Å, needed to perform the required numerical integrations and determine the corresponding equilibrium bond lengths r_e and dissociation energies D_e , we proceeded as follows. To obtain V(r) values every 0.001 Å in the r = 2.3-30.0 Å region, which excludes the innermost and outermost PEC parts defined by the 2.2-2.3 Å and 30.0-100.0 Å intervals, we used cubic splines available in LEVEL16, interpolating between pairs of nearestneighbor r values used in the ab initio electronic structure calculations, starting from (2.3 Å, 2.4



10

15

20

25

30

35

40

Å) and ending up with (25.0 Å, 30.0 Å). To generate the equally densely spaced electronic energies in the innermost and outermost segments of each of the two PECs considered in this work, we resorted to analytical potential fits provided by the LEVEL16 code. In the case of the innermost parts of the $X^1\Sigma_g^+$ and $A^1\Sigma_u^+$ potentials, corresponding to the 2.2–2.3 Å interval, we used the formula $V(r) = A + Be^{-Cr}$, where parameters A, B, and C were determined by fitting the respective electronic energies calculated at r = 2.2, 2.3, and 2.4 Å. For the outermost, 30.0–100.0 Å, PEC segments, we adopted the appropriate long-range forms of the $X^1\Sigma_g^+$ and $A^1\Sigma_u^+$ potentials, which are

$$V(r) = D_e - \sum_{m=0}^{2} C_{6+2m} / r^{6+2m}$$
(4)

in the $X^1\Sigma_g^+$ case and

$$V(r) = D_{c} - \sum_{m=0}^{5} C_{3+m} / r^{3+m}$$
 (5)

in the case of the $A^1\Sigma_u^+$ PEC. The C_6 , C_8 , and C_{10} coefficients entering the former formula were obtained by fitting the $X^1\Sigma_g^+$ electronic energies calculated at r=25.0, 30.0, and 100.0 Å to Eq. (4), in which D_e was defined as the relevant energy difference between r=100.0 Å and r_e , with r_e representing the previously determined equilibrium internuclear separation in the ground electronic state. The six coefficients C_3 through C_8 entering the latter expression were obtained by fitting the $A^1\Sigma_u^+$ electronic energies calculated at r=13.0, 15.0, 20.0, 25.0, 30.0, and 100.0 Å to Eq. (5), in which D_e was set as the energy difference between r=100.0 Å and the corresponding r_e .

The quality of the potential fits generated by LEVEL16 is very high. We illustrate it here by summarizing the results of two of the several numerical tests that we carried out for the groundstate PEC. In one of the tests, we computed the electronic energy of the $X^{1}\Sigma_{\sigma}^{+}$ state at the internuclear distance r = 3.893 Å, which is the equilibrium bond length determined by the potential fit V(r) produced by LEVEL16, using our *ab initio* quantum chemistry protocol defined by Eq. (1). The resulting energy, determined relative to the asymptotic value of the $X^1\Sigma_g^+$ potential corresponding to r = 100.0 Å, matched the value of V(r) at r = 3.893 Å obtained with LEVEL16 to within 0.0001 cm⁻¹. In another test, aimed at examining the ability of the interpolation scheme utilized by LEVEL16 to reproduce the ab initio energetics obtained using Eq. (1), we removed the electronic energies calculated at r = 4.6, 5.2, 5.8, and 6.4 Å, which is the region of the $X^1\Sigma_g^+$ PEC where V(r) changes its curvature, and regenerated the potential fit using the remaining ab initio points. The new potential fit, based on fewer ab initio energies, reproduced the equilibrium bond length $r_e = 3.893$ Å resulting from the original fit, constructed using all values of r in our grid, to within 0.001 Å (which is the step for numerical integration in LEVEL16). The mean unsigned error characterizing the $X^1\Sigma_{\sigma}^+$ energies at the removed points r = 4.6, 5.2, 5.8, and 6.4 Å resulting from the new fit relative to their ab initio values obtained using Eq. (1) was 0.05 cm⁻¹. Based on these and similar analyses, including the $X^1\Sigma_g^+$ and $A^1\Sigma_u^+$ PECs, we can safely conclude that the potential fits generated by LEVEL16 faithfully represent our ab initio data.

We also employed LEVEL16 to determine the rovibrational term values characterizing the experimentally derived analytical X-representation potential developed in (20), which we used to



10

15

20

25

30

assess the accuracy of our *ab initio* determined $X^1\Sigma_g^+$ PEC in Table 2. To be consistent with our LEVEL16 calculations for the ground-state PEC resulting from the *ab initio* protocol based on Eq. (1), we first determined the energies corresponding to the X-representation potential on the grid of 47 internuclear distances r adopted in our *ab initio* work. We then followed the same numerical procedure as described above for the $X^1\Sigma_g^+$ PEC resulting from the *ab initio* quantum chemistry calculations.

Last, but not least, we used LEVEL16 to compute the line positions of all allowed $A^1\Sigma_n^+(v', J')$ $\to X^1\Sigma_{\sigma}^+(v'', J'')$ rovibronic transitions and, with the help of our *ab initio* transition dipole moment function $\mu_z^{(X-A)}(r)$, the corresponding line intensities, as defined by the Einstein coefficients. The only adjustment that we had to make to be able to compare our calculated line positions and intensities for the allowed $A^1\Sigma_n^+(v',J') \to X^1\Sigma_\sigma^+(v'',J'')$ transitions with the LIF data reported in (20, 21) was a uniform downward shift of the entire $A^1\Sigma_u^+$ PEC resulting from our ab initio computations by 1543.2 cm⁻¹, needed to match the experimentally determined adiabatic electronic gap T_e of 26068.9 cm⁻¹ (21). Other than that, all of the calculated spectroscopic properties, including the D_e , r_e , and rovibrational term values corresponding to the $X^1\Sigma_g^+$ and $A^1\Sigma_u^+$ states and the line positions and intensities characterizing the $A^1\Sigma_u^+(v',J') \to X^1\Sigma_g^+(v'',J'')$ transitions reported in this study, rely on the raw ab initio data compiled in Tables S3-S5 and the Data S1 and S2 archives included in the Supplementary Materials (33), combined with the LEVEL16 processing, as described above. In order to produce Fig. 3, we superimposed our theoretical $A^{1}\Sigma_{n}^{+}(v'=3, J'=$ 11) $\rightarrow X^1\Sigma_g^+(v'', J'' = 10,12)$ LIF spectrum on top of the experimental one reported in Fig. 3 of (20). The theoretical line intensities shown in Fig. 3 were normalized such that the tallest peaks in the calculated and experimental LIF spectra corresponding to the v'' = 5 P12 line representing the $A^1\Sigma_{v}^+$ $(v' = 3, J' = 11) \rightarrow X^{1}\Sigma_{g}^{+}(v'' = 5, J'' = 12)$ transition match.

SUPPLEMENTARY MATERIALS

Section S1. Basis Set Convergence of the Computational Protocol Used in this Work
Section S2. Evaluating the Computational Protocol Defined by Egg. (1) and (2) by Comp

Section S2. Evaluating the Computational Protocol Defined by Eqs. (1) and (3) by Comparing the Resulting Vibrational Term Values with Experiment

Section S3. Effect of Isotopic Substitution on the $X^{1}\Sigma_{g}^{+}$ and $A^{1}\Sigma_{u}^{+}$ Rovibrational Term Values

Section S4. The Electronic Transition Dipole Moment Function Between the $X^l\Sigma_g^+$ and $A^l\Sigma_u^+$ States

Fig. S1. Comparison of the vibrational term values characterizing $^{24}\text{Mg}_2$ supported by the *ab initio* $X^1\Sigma_g^+$ and $A^1\Sigma_u^+$ potentials calculated in this work with their experimentally derived counterparts.

Fig. S2. The $X^1\Sigma_g^+ - A^1\Sigma_u^+$ electronic transition dipole moment $\mu_z^{(X-A)}(r)$ obtained in the valence full CI/A(Q+d)Z calculations for the magnesium dimer as a function of the internuclear separation r.



- Fig. S3. The $V_{J''}(r)$ effective potentials including centrifugal barriers characterizing the rotating ²⁴Mg₂ molecule at selected values of J'', along with the corresponding vibrational wave functions and information about the lifetimes for predissociation by rotation, $\tau(v'')$, characterizing quasibound states.
- Table S1. The basis set convergence of the valence correlation effects beyond CCSDT characterizing the $X^1\Sigma_g^+$ PEC of the magnesium dimer.
 - Table S2. Vibrational energies $G(v^{"})$ (in cm⁻¹) of ²⁴Mg₂ and dissociation energies D_e (in cm⁻¹) and equilibrium bond lengths r_e (in Å) of the magnesium dimer in the ground electronic state obtained in the subvalence CCSD(T) calculations correlating all electrons but the 1s shells of Mg atoms using the AwCnZ basis sets with n = T, Q, and 5, along with the corresponding CBS (T,Q) and (Q,5) extrapolations.
 - Table S3. Individual energy contributions needed to construct the $X^1\Sigma_g^+$ electronic PEC of the magnesium dimer, $E_{X^1\Sigma_g^+}$, using Eq. (1).
- Table S4. Individual energy contributions needed to construct the $A^1\Sigma_u^+$ electronic PEC of the magnesium dimer, $E_{A^1\Sigma_u^+}$, using Eq. (3).
 - Table S5. Electronic transition dipole moment between the $X^1\Sigma_g^+$ and $A^1\Sigma_u^+$ states, $\mu_z^{(X-A)}(r)$ (in Debye), as a function of the internuclear distance r (in Å).
 - Data file S1. Archive consisting of LEVEL16 outputs and spreadsheets containing detailed information about the rovibrational states supported by the $X^1\Sigma_g^+$ and $A^1\Sigma_u^+$ potentials calculated in this work, along with the associated README S1.txt file.
 - Data file S2. Archive consisting of LEVEL16 outputs containing detailed information about the $A^1\Sigma_u^+(v',J') \to X^1\Sigma_g^+(v'',J'')$ rovibronic transitions calculated in this work, along with the associated README S2.txt file.



10

15

30

REFERENCES AND NOTES

- 1. J.-C. Zhang, J.-F. Sun, Z.-L. Zhu, Y.-F. Liu, Elastic collision properties of ultracold calcium atoms. *Phys. Scr.* **87**, 025302 (2013).
- 2. E. Krotscheck, R. E. Zillich, Solvation of Mg in helium-4: Are there meta-stable Mg dimers? *J. Chem. Phys.* **145**, 244317 (2016).
- 3. L. Rybak, S. Amaran, L. Levin, M. Tomza, R. Moszynski, R. Kosloff, C. P. Koch, Z. Amitay, Generating molecular rovibrational coherence by two-photon femtosecond photoassociation of thermally hot atoms. *Phys. Rev. Lett.* **107**, 273001 (2011).
- 4. P. Wolf, P. Lemonde, A. Lambrecht, S. Bize, A. Landragin, A. Clairon, From optical lattice clocks to the measurement of forces in the Casimir regime. *Phys. Rev. A* **75**, 063608 (2007).
- 5. C. Simon, D. Jaksch, Possibility of observing energy decoherence due to quantum gravity. *Phys. Rev. A* **70**, 052104 (2004).
- 6. M. Machholm, P. S. Julienne, K.-A. Suominen, Calculations of collisions between cold alkaline-earth-metal atoms in a weak laser field. *Phys. Rev. A* **64**, 033425 (2001).
- 7. P. F. Bernath, Extracting potentials from spectra. *Science* **324**, 1526–1527 (2009).
 - 8. K. Patkowski, V. Špirko, K. Szalewicz, On the elusive twelfth vibrational state of beryllium dimer. *Science* **326**, 1382–1384 (2009).
 - 9. I. Magoulas, N. P. Bauman, J. Shen, P. Piecuch, Application of the CC(*P*;*Q*) hierarchy of coupled-cluster methods to the beryllium dimer. *J. Phys. Chem. A* **122**, 1350–1368 (2018).
- 10. V. V. Meshkov, A. V. Stolyarov, M. C. Heaven, C. Haugen, R. J. Le Roy, Direct-potential-fit analyses yield improved empirical potentials for the ground X¹Σ_g⁺ state of Be₂. *J. Chem. Phys.* 140, 064315 (2014).
 - 11. J. M. Merritt, V. E. Bondybey, M. C. Heaven, Beryllium dimer–caught in the act of bonding. *Science* **324**, 1548–1551 (2009).
- 12. W. J. Balfour, A. E. Douglas, Absorption spectrum of the Mg₂ molecule. *Can. J. Phys.* 48, 901–914 (1970).
 - 13. R. Rydberg, Graphische Darstellung einiger bandenspektroskopischer Ergebnisse. *Z. Phys.* **73**, 376–385 (1932).
 - 14. R. Rydberg, Über einige Potentialkurven des Quecksilberhydrids. Z. Phys. **80**, 514–524 (1933).
 - 15. O. Klein, Zur Berechnung von Potentialkurven für zweiatomige Moleküle mit Hilfe von Spektraltermen. Z. Phys. **76**, 226–235 (1932).
 - 16. A. L. G. Rees, The calculation of potential-energy curves from band-spectroscopic data. *Proc. Phys. Soc.* **59**, 998–1008 (1947).
- 17. K. C. Li, W. C. Stwalley, Vibrational levels near dissociation in Mg₂ and long-range forces. *J. Chem. Phys.* **59**, 4423–4427 (1973).
 - 18. W. C. Stwalley, Long-range analysis of the internuclear potential of Mg₂. *Chem. Phys. Lett.* **7**, 600–602 (1970).



15

20

25

- 19. W. C. Stwalley, Polarizability and long-range interactions of magnesium atoms. *J. Chem. Phys.* **54**, 4517–4518 (1971).
- 20. H. Knöckel, S. Rühmann, E. Tiemann, The $X^1\Sigma_g^+$ ground state of Mg₂ studied by Fourier-transform spectroscopy. *J. Chem. Phys.* **138**, 094303 (2013); **138**, 189901 (2013) [Erratum].
- 5 21. H. Knöckel, S. Rühmann, E. Tiemann, The $A^{1}\Sigma_{u}^{+} + (1)^{1}\Pi_{u}$ system of Mg₂. *Eur. Phys. J. D* **68**, 293 (2014).
 - 22. H. Scheingraber, C. R. Vidal, Discrete and continuous Franck Condon factors of the Mg₂ $A^1\Sigma_n^+ X^1\Sigma_n^+$ system and their *J* dependence. *J. Chem. Phys.* **66**, 3694–3704 (1977).
 - 23. S. G. Porsev, A. Derevianko, High-accuracy relativistic many-body calculations of van der Waals coefficients C_6 for alkaline-earth-metal atoms. *Phys. Rev. A* **65**, 020701(R) (2002).
 - 24. S. G. Porsev, A. Derevianko, High-accuracy calculations of dipole, quadrupole, and octupole electric dynamic polarizabilities and van der Waals coefficients C₆, C₈, and C₁₀ for alkaline-earth dimers. *J. Exp. Theor. Phys.* **102**, 195–205 (2006).
 - 25. W. J. Balfour, R. F. Whitlock, Rotational dependence of Franck-Condon factors in the $A^1\Sigma_u^+$ $\leftarrow X^1\Sigma_g^+$ system of ²⁴Mg₂. *Can. J. Phys.* **50**, 1648–1651 (1972).
 - 26. S. H. Yuwono, I. Magoulas, J. Shen, P. Piecuch, Application of the coupled-cluster CC(*P*;*Q*) approaches to the magnesium dimer. *Mol. Phys.* **117**, 1486–1506 (2019).
 - 27. E. Tiesinga, S. Kotochigova, P. S. Julienne, Scattering length of the ground-state Mg + Mg collision. *Phys. Rev. A* **65**, 042722 (2002).
 - 28. J. Čížek, On the correlation problem in atomic and molecular systems. Calculation of wavefunction components in Ursell-type expansion using quantum-field theoretical methods. *J. Chem. Phys.* **45**, 4256–4266 (1966).
 - 29. S. Amaran, R. Kosloff, M. Tomza, W. Skomorowski, F. Pawłowski, R. Moszynski, L. Rybak, L. Levin, Z. Amitay, J. M. Berglund, D. M. Reich, C. P. Koch, Femtosecond two-photon photoassociation of hot magnesium atoms: A quantum dynamical study using thermal random phase wavefunctions. *J. Chem. Phys.* **139**, 164124 (2013).
 - 30. K. Patkowski, R. Podeszwa, K. Szalewicz, Interactions in diatomic dimers involving closed-shell metals. *J. Phys. Chem. A* **111**, 12822–12838 (2007).
 - 31. H. Li, H. Feng, W. Sun, Y. Zhang, Q. Fan, K. A. Peterson, Y. Xie, H. F. Schaefer, III, The alkaline earth dimer cations (Be₂⁺, Mg₂⁺, Ca₂⁺, Sr₂⁺, and Ba₂⁺). Coupled cluster and full configuration interaction studies. *Mol. Phys.* **111**, 2292–2298 (2013).
 - 32. K. Raghavachari, G. W. Trucks, J. A. Pople, M. Head-Gordon, A fifth-order perturbation comparison of electron correlation theories. *Chem. Phys. Lett.* **157**, 479–483 (1989).
 - 33. Supplementary Materials to the present article.
- 34. H. J. Monkhorst, Calculation of properties with the coupled-cluster method. *Int. J. Quantum Chem.*, *Symp.* **11**, 421–432 (1977).
 - 35. J. Noga, R. J. Bartlett, The full CCSDT model for molecular electronic structure. *J. Chem. Phys.* **86**, 7041–7050 (1987); **89**, 3401 (1988) [Erratum].



10

15

25

30

35

- 36. G. E. Scuseria, H. F. Schaefer, III, A new implementation of the full CCSDT model for molecular electronic structure. *Chem. Phys. Lett.* **152**, 382–386 (1988).
- 37. J. F. Stanton, R. J. Bartlett, The equation of motion coupled-cluster method. A systematic biorthogonal approach to molecular excitation energies, transition probabilities, and excited state properties. *J. Chem. Phys.* **98**, 7029–7039 (1993).
- 38. K. Kowalski, P. Piecuch, The active-space equation-of-motion coupled-cluster methods for excited electronic states: Full EOMCCSDt. *J. Chem. Phys.* **115**, 643–651 (2001).
- 39. S. A. Kucharski, M. Włoch, M. Musiał, R. J. Bartlett, Coupled-cluster theory for excited electronic states: The full equation-of-motion coupled-cluster single, double, and triple excitation method. *J. Chem. Phys.* **115**, 8263–8266 (2001).
- 40. K. Kowalski, P. Piecuch, New coupled-cluster methods with singles, doubles, and noniterative triples for high accuracy calculations of excited electronic states. *J. Chem. Phys.* **120**, 1715–1738 (2004).
- 41. B. P. Prascher, D. E. Woon, K. A. Peterson, T. H. Dunning, Jr., A. K. Wilson, Gaussian basis sets for use in correlated molecular calculations. VII. Valence, core-valence, and scalar relativistic basis sets for Li, Be, Na, and Mg. *Theor. Chem. Acc.* **128**, 69–82 (2011).
- 42. K. A. Peterson, Correlation consistent basis sets. tyr0.chem.wsu.edu/~kipeters/basis.html.
- 43. T. Helgaker, W. Klopper, H. Koch, J. Noga, Basis-set convergence of correlated calculations on water. *J. Chem. Phys.* **106**, 9639–9646 (1997).
- 44. P. Piecuch, J. A. Hansen, A. O. Ajala, Benchmarking the completely renormalised equation-of-motion coupled-cluster approaches for vertical excitation energies. *Mol. Phys.* **113**, 3085–3127 (2015).
 - 45. C. R. Vidal, H. Scheingraber, Determination of diatomic molecular constants using an inverted perturbation approach: Application to the $A^1\Sigma_u^+ X^1\Sigma_g^+$ system of Mg₂. J. Mol. Spectrosc. 65, 46–64 (1977).
 - 46. M. Douglas, N. M. Kroll, Quantum electrodynamical corrections to the fine structure of helium. *Ann. Phys.* **82**, 89–155 (1974).
 - 47. T. Nakajima, K. Hirao, The Douglas-Kroll-Hess approach. Chem. Rev. 112, 385-402 (2012).
 - 48. M. S. Gordon, M. W. Schmidt, Eds., C. E. Dykstra, G. Frenking, K. S. Kim, G. E. Scuseria, in *Theory and Applications of Computational Chemistry: The First Forty Years* (Elsevier, Amsterdam, 2005), pp. 1167–1189.
 - 49. M. Valiev, E. J. Bylaska, N. Govind, K. Kowalski, T. P. Straatsma, H. J. J. Van Dam, D. Wang, J. Nieplocha, E. Apra, T. L. Windus, W. A. de Jong, NWChem: A comprehensive and scalable open-source solution for large scale molecular simulations. *Comput. Phys. Commun.* **181**, 1477–1489 (2010).
 - 50. P. Piecuch, S. A. Kucharski, K. Kowalski, M. Musiał, Efficient computer implementation of the renormalized coupled-cluster methods: The R-CCSD[T], R-CCSD(T), CR-CCSD[T], and CR-CCSD(T) approaches. *Comp. Phys. Commun.* **149**, 71–96 (2002).
 - 51. J. W. Cooley, An improved eigenvalue corrector formula for solving the Schrödinger equation for central fields. *Math. Comput.* **15**, 363–374 (1961).



- 52. R. J. Le Roy, LEVEL: A computer program for solving the radial Schrödinger equation for bound and quasibound levels. *J. Quant. Spectrosc. Radiat. Transf.* **186**, 167–178 (2017).
- 53. R. J. Le Roy, R. B. Bernstein, Shape resonances and rotationally predissociating levels: The atomic collision time-delay functions and quasibound level properties of $H_2(X^l\Sigma_g^+)$. *J. Chem. Phys.* **54**, 5114–5126 (1971).

Acknowledgments:

5

10

15

20

Funding: This work has been supported by the Chemical Sciences, Geosciences and Biosciences Division, Office of Basic Energy Sciences, Office of Science, U.S. Department of Energy (Grant No. DE-FG02-01ER15228) and National Science Foundation (Grant No. CHE-1763371). Author contributions: I.M. and P.P. conceived the project; S.H.Y. and I.M. performed the electronic structure calculations under P.P.'s supervision; S.H.Y. carried out the rovibrational analysis and computed the rovibronic spectrum, which was subsequently used to simulate the relevant LIF spectra; All authors contributed equally and extensively to the discussion and interpretation of the data; All authors worked closely together on preparing the manuscript; P.P. supervised the entire project. Competing interests: Authors declare no competing interests. Data and materials availability: All data supporting the content and conclusions of this work are included in the main text and the Supplementary Materials. Any additional information can be obtained from the authors upon request.

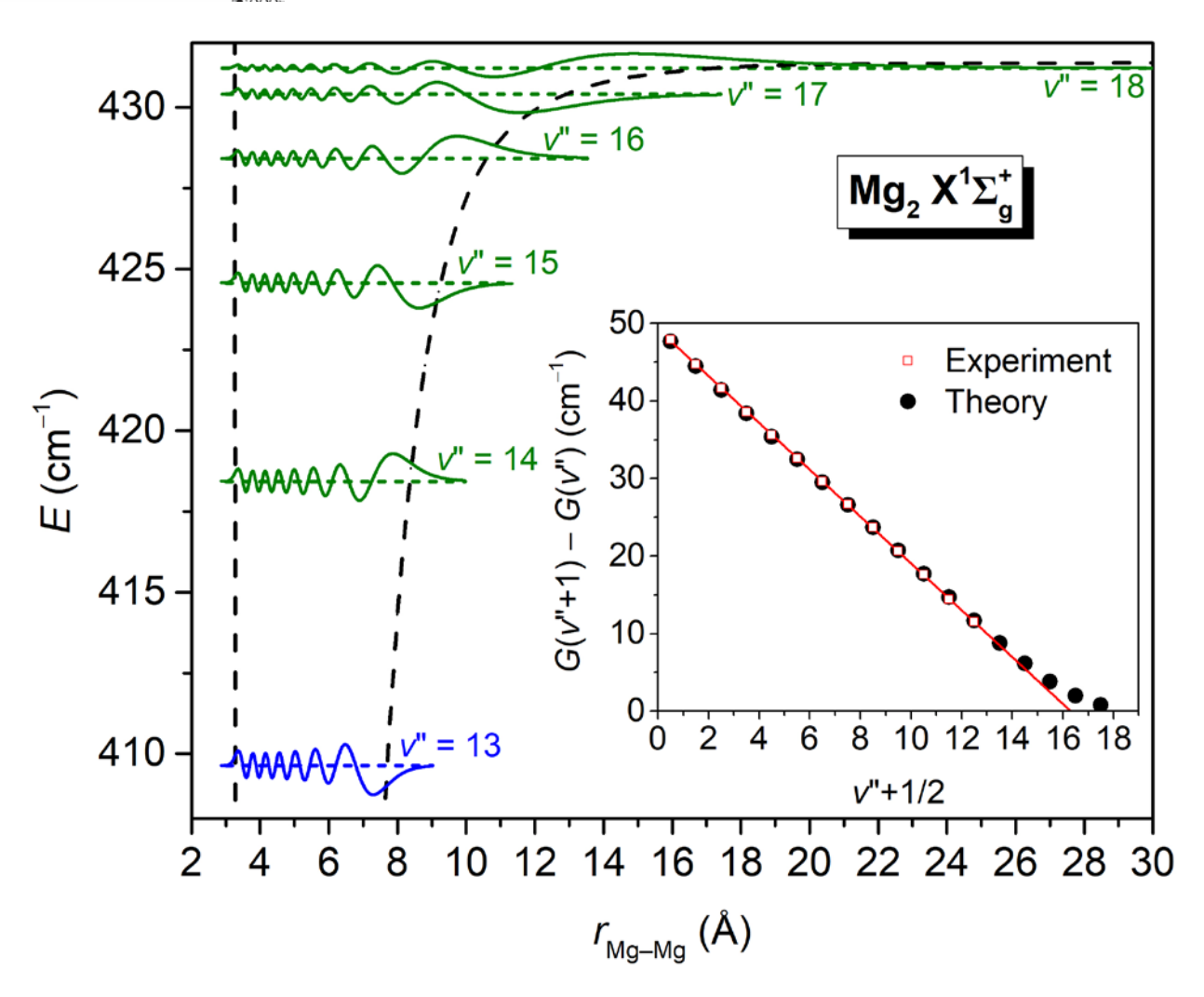


Fig. 1. The wave functions of the high-lying, purely vibrational, states of 24 Mg₂ and the underlying $X^1\Sigma_g^+$ potential. The last experimentally observed v'' = 13 level is marked in blue, the predicted v'' = 14—18 levels are marked in green, and the *ab initio* $X^1\Sigma_g^+$ PEC obtained in this study is marked by a long-dashed black line. The inset is a Birge–Sponer plot comparing the rotationless G(v'' + 1) - G(v'') energy differences as functions of $v'' + \frac{1}{2}$ obtained in this work (black circles) with their experimentally derived counterparts (red open squares) based on the data reported in (12) (v'' = 0—12) and (17) (v'' = 13; *cf.*, also, Table 1). The red solid line is a linear fit of the experimental points.



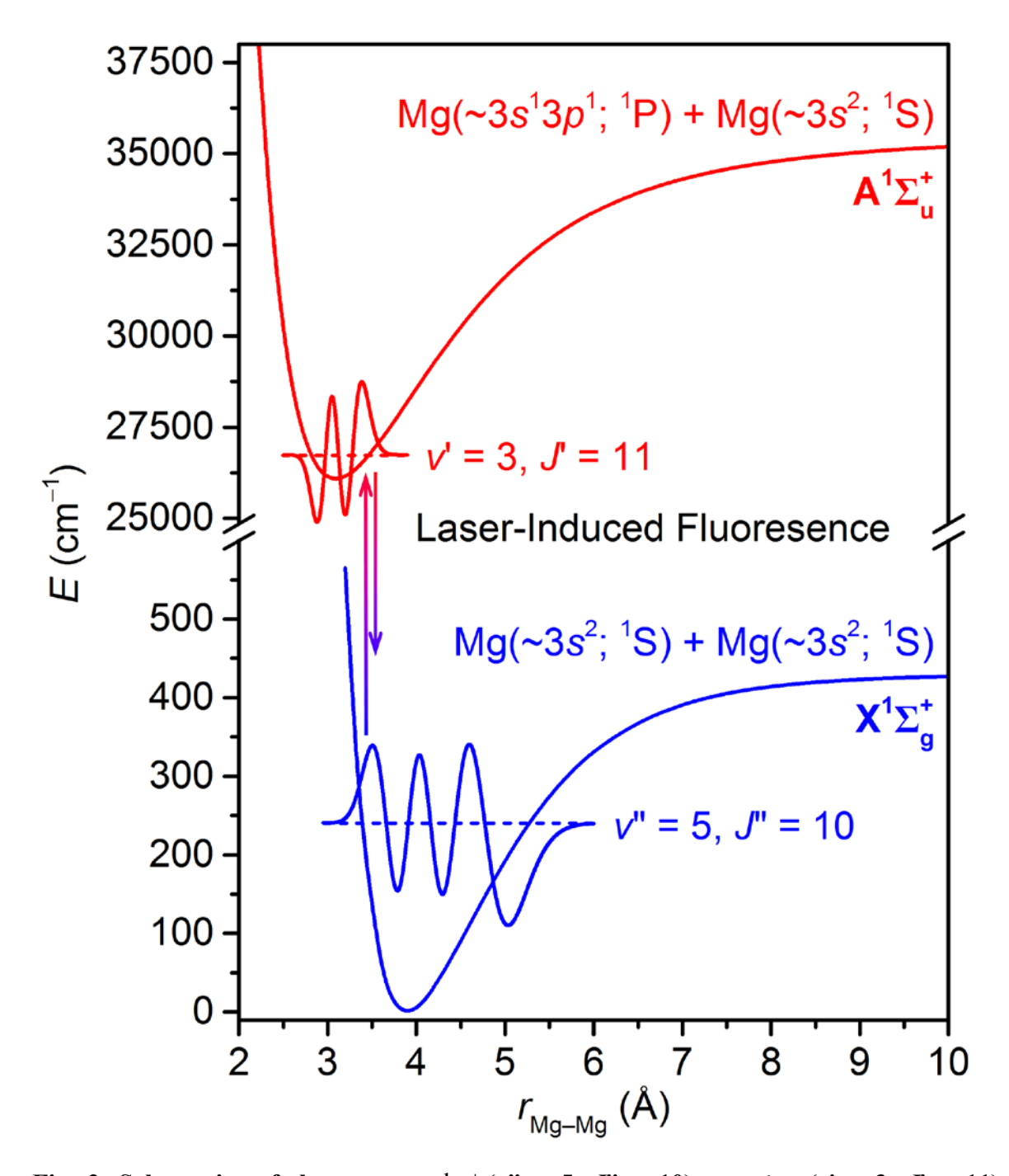


Fig. 2. Schematics of the pump, $X^1\Sigma_g^+$ (v''=5, J''=10) $\to A^1\Sigma_u^+$ (v'=3, J'=11), and fluorescence, $A^1\Sigma_u^+$ (v'=3, J'=11) $\to X^1\Sigma_g^+$ (v'', J''=10,12), processes resulting in the LIF spectrum for ²⁴Mg₂ shown in Fig. 3 of (20). The $X^1\Sigma_g^+$ and $A^1\Sigma_u^+$ PECs and the corresponding $X^1\Sigma_g^+$ (v''=5, J''=10) and $A^1\Sigma_u^+$ (v'=3, J'=11) rovibrational wave functions were calculated in this work. The $A^1\Sigma_u^+$ PEC was shifted to match the experimentally determined adiabatic electronic excitation energy T_e of 26068.9 cm⁻¹ (21) (see the Materials and Methods section for the details).



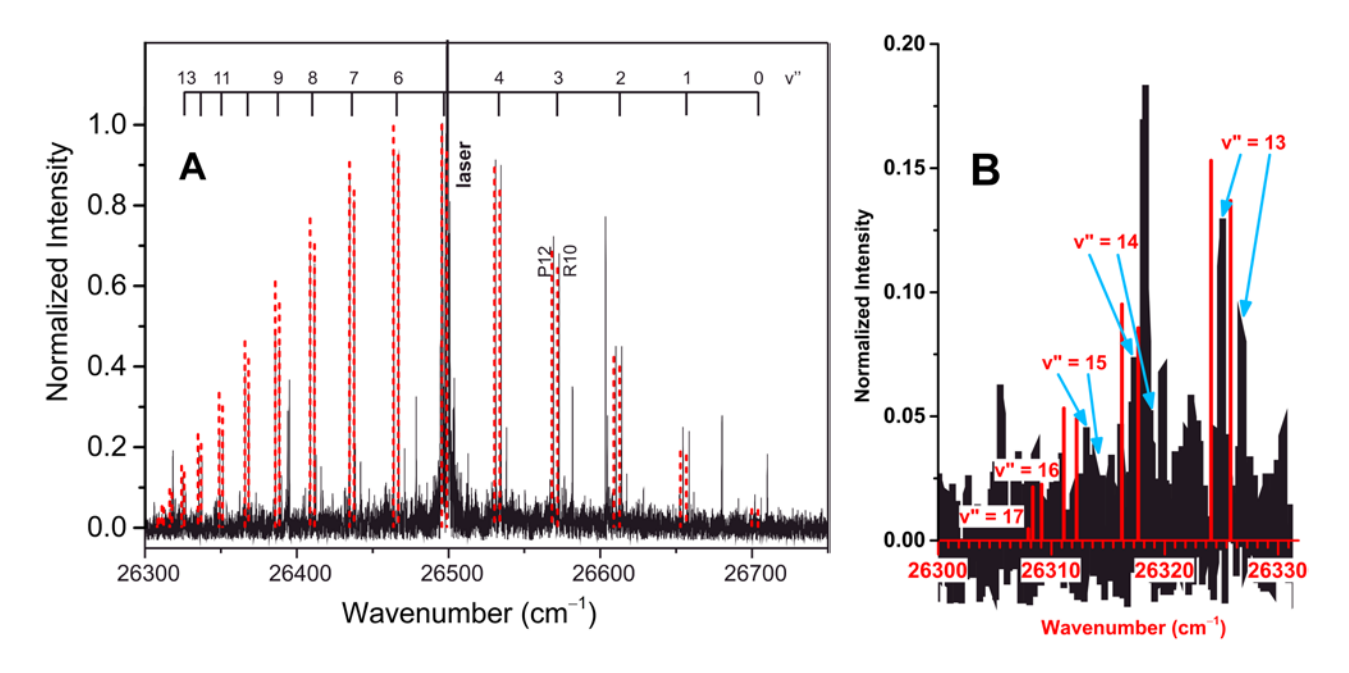


Fig. 3. The $A^1\Sigma_u^+$ (v'=3, J'=11) $\to X^1\Sigma_g^+$ (v'', J''=10,12) LIF spectrum of $^{24}Mg_2$. (A) Comparison of the experimental $A^1\Sigma_u^+$ (v'=3, J'=11) $\to X^1\Sigma_g^+$ (v'', J''=10,12) fluorescence progression (black solid lines; adapted from Fig. 3 of (20) with the permission of AIP Publishing) with its *ab initio* counterpart obtained in this work (red dashed lines). The theoretical line intensities were normalized such that the tallest peaks in the calculated and experimental spectra corresponding to the v''=5 P12 line match. (B) Magnification of the low-energy region of the LIF spectrum shown in (A), with red solid lines representing the calculated transitions. The blue arrows originating from the v''=13 label indicate the location of the experimentally observed v''=13 P12/R10 doublet. The blue arrows originating from the v''=14 and 15 labels point to the most probable locations of the corresponding P12/R10 doublets. Spectral lines involving v''=16 and 17 are buried in the noise (see, also, Table 3).



10

Table 1. Comparison of the *ab initio* (Calc.) and experimentally derived (Expt.) rovibrational G(v'', J'') energies for selected values of J'' characterizing ²⁴Mg₂ in the ground electronic state (in cm⁻¹), along with the corresponding dissociation energies D_e (in cm⁻¹) and equilibrium bond lengths r_e (in Å). The G(v'', J'') energies calculated using the *ab initio* $X^1\Sigma_g^+$ PEC defined by Eq. (1) are reported as errors relative to experiment, whereas D_e and r_e are the actual values of these quantities. If the experimental G(v'', J'') energies are not available, we provide their calculated values in square brackets. Quasi-bound rovibrational levels are given in italics. Horizontal bars indicate term values not supported by the $X^1\Sigma^+_{\sigma}$ PEC.

ν"	G(v", J" = 0)	G(v", J" = 20)	G(v", J" = 40)	G(v", J" = 60)	G(v'', J'' = 80)	
	Calc. Expt. ^a	Calc. Expt.b	Calc. Expt.b	Calc. Expt.b	Calc. Expt.b	
0	0.0 25.2	-0.2 63.3	-0.4 171.2	-0.9 340.4	-1.8 <i>552.8</i>	
1	-0.2 73.0	-0.4 109.7	-0.7 213.1	-1.2 374.6	-2.2 573.2	
2	-0.5 117.8	-0.7 153.0	-1.0 252.0	-1.6 405.4	[585.0]	
3	-0.7 159.4	-1.0 193.2	-1.3 287.7	-1.9 <i>432.9</i>	_	
4	-0.9 198.0	-1.3 230.3	-1.6 320.3	-2.1 <i>456.7</i>	_	
5	-1.1 233.6	-1.5 264.4	-1.8 349.7	-2.1 476.5	_	
6	-1.2 266.2	-1.7 295.5	-1.9 375.9	-1.7 <i>491.7</i>	_	
7	-1.3 295.8	-1.8 323.6	-1.9 398.8	_	_	
8	-1.4 322.5	-1.7 348.5	-1.7 418.1	_	_	
9	-1.4 346.2	-1.6 370.3	-1.4 <i>433</i> .9		_	
10	-1.3 366.8	-1.4 389.0	[444.5]	_	_	
11	-1.2 384.4	-1.2 404.4	[451.6]		_	
12	-0.9 398.8	-0.9 416.6	_	_	_	
13	-0.7 410.3	-0.5 425.5	_	_	_	
14	[418.4]	[431.1]	_		_	
15	[424.6]	_	_		_	
16	[428.4]	_	_		_	
17	[430.4]	_	_		_	
18	[431.2]	_	<u> </u>	_		
D_{e}	431.4 430.472	e				

3.893 3.89039° $r_{\rm e}$

^aExperimentally derived values for v'' = 0–12 taken from (12). The v'' = 13 value is calculated as G(v'' = 13, J'' = 14) - 210B(v'' = 13, J'' = 14) with the information about G(v'' = 13, J'' = 14) and B(v'' = 13, J'' = 14) taken from (17). Experimentally derived values taken from the Supplementary Material of (21). Experimentally derived values taken from (20, 21) assuming the Xrepresentation of the $X^{l}\Sigma_{g}^{+}$ potential developed in (20).



Table 2. Comparison of the rovibrational G(v", J") energies obtained using the *ab initio* $X^1\Sigma_g^+$ PEC defined by Eq. (1) (Calc.) and its X-representation counterpart constructed in (20) (X-rep.) for selected values of J" characterizing 24 Mg₂ in the ground electronic state (in cm⁻¹), along with the corresponding dissociation energies D_e (in cm⁻¹) and equilibrium bond lengths r_e (in Å). The G(v", J") energies calculated using the *ab initio* $X^1\Sigma_g^+$ PEC are reported as errors relative to the X-representation data, whereas D_e and r_e are the actual values of these quantities. If a given G(v", J") state corresponding to our *ab initio* $X^1\Sigma_g^+$ PEC is not supported by the X-representation potential of (20), we provide its energy in square brackets. Quasi-bound rovibrational levels are given in italics. Horizontal bars indicate term values not supported by the $X^1\Sigma_g^+$ PEC.

ν"	G(v", J" = 0)		G(v", J)	J'' = 20)	G(v'', J)	7" = 40)	$G(v", \omega)$	/ " = 60)	$G(v", \omega)$	7" = 80)
	Calc.	X-rep.	Calc.	X-rep.	Calc.	X-rep.	Calc.	X-rep.	Calc.	X-rep.
0	-0.1	25.2	-0.2	63.3	-0.4	171.2	-0.9	340.4	-1.8	552.8
1	-0.3	73.1	-0.4	109.7	-0.7	213.1	-1.2	374.6	-2.2	573.2
2	-0.6	117.9	-0.7	153.0	-1.0	252.0	-1.6	405.4	[58	5.0]
3	-0.9	159.6	-1.0	193.2	-1.3	287.7	-1.9	432.9	-	_
4	-1.1	198.2	-1.2	230.3	-1.6	320.3	-2.1	456.7	_	
5	-1.4	233.9	-1.5	264.4	-1.8	349.7	-2.1	476.5	-	_
6	-1.5	266.5	-1.6	295.5	-1.9	375.9	-1.7	491.7	-	_
7	-1.7	296.2	-1.7	323.5	-1.9	398.8	_		_	
8	-1.7	322.8	-1.7	348.5	-1.7	418.1			_	
9	-1.6	346.4	-1.6	370.3	-1.4	433.8	_		_	
10	-1.5	367.0	-1.4	389.0	-1.0	445.5	_		_	
11	-1.3	384.5	-1.2	404.4	[451.6]		_		_	
12	-1.0	399.0	-0.9	416.6	_		_		_	
13	-0.7	410.4	-0.5	425.5	_		_		-	_
14	-0.5	418.9	-0.2	431.2	_		_		-	_
15	-0.2	424.7	_	_	-	_	-	_	-	_
16	0.2	428.3	-	_	_		-	_		_
17	0.5	429.9	-	_	_		_		-	_
18	0.8	430.4								
D_{e}	431.4	430.472								
<i>r</i> e	3.893	3.89039								



Table 3. Comparison of the theoretical line positions of the $A^1\Sigma_u^+(v'=3, J=11) \to X^1\Sigma_g^+(v'', J''=10,12)$ fluorescence progression in the LIF spectrum of $^{24}\text{Mg}_2$ calculated in this work with experiment. All line positions are in cm⁻¹. The available experimental values are the actual line positions, whereas our calculated results are errors relative to experiment. If the experimentally determined line positions are not available, we provide their calculated values in square brackets. Horizontal bars indicate term values not supported by the $X^1\Sigma_g^+$ PEC.

		P12		R10		
v"	Calc.	Expt. ^a	Calc.	Expt. ^a		
0	-1.5	26701.9	-1.5	26706.0		
1	-1.2	26654.5	-1.3	26658.5		
2	-1.0	26610.3	-1.0	26614.1		
3	-0.7	26569.2	-0.7	26572.8		
4	-0.4	26531.1	-0.5	26534.6		
5	-0.2	26496.0	-0.2	26499.3 ^b		
6	0.0	0.0 26463.9		[26467.1]		
7	0.1	26434.9	0.1	26437.9		
8	0.1	26408.8	0.1	26411.7		
9	0.0	26385.9	0.0	26388.5		
10	-0.2	26366.0	-0.2	26368.4		
11	-0.4	26349.2	-0.4	26351.4		
12	-0.7	26335.6	-0.6	26337.5		
13	-1.0	26325.0	-0.9	26326.7		
14	[26	[26316.2]		[26317.7]		
15	[26	[26311.1]		[26312.2]		
16	[26	[26308.4]		[26309.1]		
17		_		[26308.0]		
18						

^aDifferences between the experimental $X^1\Sigma_g^+(v'', J''=10,12)$ and $A^1\Sigma_u^+(v'=3, J'=11)$ term values reported in the Supplementary Material of (21) (see (33)), unless stated otherwise. ^bThe $X^1\Sigma_g^+(v''=5, J''=10) \rightarrow A^1\Sigma_u^+(v'=3, J'=11)$ pump frequency reported in Fig. 3 of (20).